

Direct Imaging Search for Extrasolar Planets in the Pleiades

Kodai YAMAMOTO¹, Taro MATSUO², Hiroshi SHIBAI¹, Yoichi ITOH³, Mihoko KONISHI¹,
Jun SUDO¹, Ryoko TANI⁴, Misato FUKAGAWA¹, Takahiro SUMI¹, Tomoyuki KUDO⁵,
Jun HASHIMOTO⁶, Nobuhiko KUSAKABE⁶, Lyu ABE⁷, Wolfgang BRANDNER⁸,
Timothy D. BRANDT⁹, Joseph CARSON¹⁰, Thayne CURRIE¹¹, Sebastian E. EGNER⁵,
Markus FELDT⁸, Miwa GOTO⁸, Carol GRADY¹², Olivier GUYON⁵, Yutaka HAYANO⁵,
Masahiko HAYASHI¹³, Saeko HAYASHI⁵, Thomas HENNING⁸, Klaus HODAPP¹⁴, Miki ISHII⁵,
Masanori IYE⁶, Markus JANSON⁹, Ryo KANDORI⁶, Gillian R. KNAPP⁹,
Masayuki KUZUHARA⁶, Jungmi KWON¹⁵, ⁶ Mike McELWAIN¹⁶, Shoken MIYAMA¹⁷,
Jun-Ichi MORINO⁶, Amaya MORO-MARTIN¹⁸, June NISHIKAWA⁶, Tetsuo NISHIMURA⁵,
Tae-Soo PYO⁵, Eugene SERABYN¹⁹, Hiroshi SUTO⁶, Ryuji SUZUKI²⁰, Michihiro TAKAMI²¹,
Naruhisa TAKATO⁵, Hiroshi TERADA⁵, Christian THALMANN⁸, Daigo TOMONO⁵,
Edwin L. TURNER¹⁰, John WISNIEWSKI²², Makoto WATANABE²³, Toru YAMADA²⁴,
Hideki TAKAMI⁵, Tomonori USUDA⁵, and Motohide TAMURA⁶

¹*Department of Earth and Space Science, Graduate School of Science, Osaka University, 1-1
Machikaneyama, Toyonaka, Osaka 560-0043, Japan*

yamamoto@iral.ess.sci.osaka-u.ac.jp

shibai@iral.ess.sci.osaka-u.ac.jp

konishi@iral.ess.sci.osaka-u.ac.jp

sudo@iral.ess.sci.osaka-u.ac.jp

misato@iral.ess.sci.osaka-u.ac.jp

sumi@iral.ess.sci.osaka-u.ac.jp

²*Department of Astronomy, Faculty of Science, Kyoto University, Kitashirakawa-Oiwake-cho,
Sakyo-ku, Kyoto 606-8502, Japan*

matsuo@kusastro.kyoto-u.ac.jp

³*Nishi-Harima Astronomical Observatory, 407-2 Nishigaichi, Sayo-cho, Sayo-gun, Hyogo 679-5313,
Japan*

yitoh@nhao.jp

⁴*Graduate School of Science, Kobe University, 1-1 Rokkodai, Nada, Kobe, Hyogo 657-8501, Japan*

⁵*Subaru Telescope, 650 North Aohoku Place, Hilo, HI 96720, USA*

⁶*National Astronomical Observatory of Japan, 2-21-1 Osawa, Mitaka, Tokyo 181-8588, Japan*

motohide.tamura@nao.jp

⁷*Laboratoire Lagrange, UMR7293, Université de Nice-Sophia Antipolis, CNRS, Observatoire de la
Côte d'Azur, 06300 Nice, France*

⁸*Max Planck Institute for Astronomy, Heidelberg, Germany*

⁹*Department of Astrophysical Sciences, Princeton University, NJ 08544, USA*

¹⁰*Department of Physics and Astronomy, College of Charleston, 58 Coming St., Charleston, SC 29424, USA*

¹¹*Department of Astronomy and Astrophysics, University of Toronto, 27 King's College Circle, Toronto, Ontario, Canada M5S 1A1*

¹²*Eureka Scientific, 2452 Delmer, Suite 100, Oakland CA 96002, USA*

¹³*Department of Astronomy, The University of Tokyo, Hongo 7-3-1, Bunkyo-ku, Tokyo 113-0033, Japan*

¹⁴*Institute for Astronomy, University of Hawaii, 640 North A'ohoku Place, Hilo, HI 96720, USA*

¹⁵*Department of Astronomical Science, The Graduate University for Advanced Studies (SOKENDAI), 2-21-1 Osawa, Mitaka, Tokyo 181-8588, Japan*

¹⁶*ExoPlanets and Stellar Astrophysics Laboratory, Code 667, Goddard Space Flight Center, Greenbelt, MD 20771, USA*

¹⁷*Office of the President, Hiroshima University, 1-3-2 Kagamiyama, Higashi-Hiroshima, 739-8511, Japan*

¹⁸*Departamento de Astrofísica, CAB (INTA-CSIC), Instituto Nacional de Técnica Aeroespacial, Torrejón de Ardoz, 28850, Madrid, Spain*

¹⁹*Jet Propulsion Laboratory, California Institute of Technology, Pasadena, CA, USA*

²⁰*TMT Observatory Corporation, 1111 South Arroyo Parkway, Pasadena, CA 91105, USA*

²¹*Institute of Astronomy and Astrophysics, Academia Sinica, P.O. Box 23-141, Taipei 106, Taiwan*

²²*Department of Astronomy, University of Washington, Box 351580 Seattle, WA 98195, USA*

²³*Department of CosmoSciences, Hokkaido University, Sapporo 060-0810, Japan*

²⁴*Astronomical Institute, Tohoku University, Aoba, Sendai 980-8578, Japan*

(Received ; accepted)

Abstract

We carried out an imaging survey for extrasolar planets around stars in the Pleiades (125 Myr, 135 pc) in the H and K_S bands using HiCIAO combined with the adaptive optics, AO188, on the Subaru telescope. We found 13 companion candidates fainter than 14.5 mag in the H band around 9 stars. Five of these 13 were confirmed to be background stars by measurement of their proper motion. One was not found in the second epoch observation, and thus was not a background or companion object. One had multi-epoch image, but the precision of its proper motion was not sufficient to conclude whether it was background object. Four other candidates are waiting for second epoch observations to determine their proper motion. Finally, the remaining 2 were confirmed to be $60 M_J$ brown dwarf companions orbiting around HD 23514 (G0) and HII 1348 (K5) respectively, as had been reported in previous

studies. In our observations, the average detection limit for a point source was 20.3 mag in the H band beyond $1''.5$ from the central star. On the basis of this detection limit, we calculated the detection efficiency to be 90% for a planet with 6 to 12 Jovian masses and a semi-major axis of 50–1000 AU. For this we extrapolated the distribution of planet mass and semi-major axis derived from RV observations and adopted the planet evolution model of Baraffe et al. (2003). As there was no detection of a planet, we estimated the frequency of such planets to be less than 17.9% (2σ) around one star of the Pleiades cluster.

Key words: infrared: stars — methods: statistical — stars: low-mass, brown dwarfs — stars: planetary systems — techniques: high angular resolution

1. Introduction

Understanding planet-building and their evolutionary process is one of the most challenging problems in astrophysics. Theoretically, there have been two main competing hypotheses regarding the formation of gas-giant planets: core accretion (e.g., Safronov 1969; Mizuno 1980; Pollack et al. 1996) and disk instability (e.g., Kuiper 1951; Cameron 1978). Planet formation theories have been continuously updated or newly proposed (e.g., Inutsuka et al. 2010), but these two hypotheses have served as the basis for most studies. On the one hand, in the core accretion model, relatively small giant planets such as Jupiter and Saturn are thought to form at about 10 AU or less from a solar-type host star in several Myr (Pollack et al. 1996; Ida & Lin 2004). On the other hand, in the disk instability model, planets of a few to $10 M_J$ can be created within a few 10 to 100 AU from the central star on a dynamical timescale of several thousand years (Rafikov 2007; Rafikov 2011; Marois et al. 2008; Kratter et al. 2010; Janson et al. 2012). These formation models therefore predict two populations of giant planets segregated by orbital distance, with the closer planets formed by core accretion and the outer ones by disk instability.

However, planets may experience subsequent orbital migration as a result of interaction with the parent disk either inward or even outward in the case of type III migration (Masset & Papaloizou 2003). Furthermore, in a system with multiple planets, one can be ejected beyond the outer radius of the disk through gravitational interaction between planets or their embryos (e.g. Ida & Lin 2004; Veras et al. 2009; Basu & Vorobyov 2012). In addition, free-floating planets might be captured at wide orbits, although such widely separated planets are likely rare (on the order of a few percent, e.g., Kouwenhoven et al. 2010). Thus, a number of mechanisms to explain the formation and evolution of planets have been theoretically explored, but it is most important to observationally determine planet frequency over a wide range of orbital distances.

Observationally, more than 830 extrasolar planets have been found to date, of which about 90% were detected by radial velocity (RV) and transit observations (e.g. Mayor et al.

2011; Howard et al. 2010). This rapidly growing sample allows a statistical discussion of planet frequency based on the properties of the planets and their host stars. However, these observing methods have a limitation: it is difficult to detect planets that are far from host stars, i.e., more than about 10 AU. Direct imaging, however, which is sensitive to such distant regions, can provide critical and complementary information to that obtained by indirect detection methods (Marois et al. 2008; Marois et al. 2010; Lagrange et al. 2010; Currie et al. 2011; Carson et al. 2012). Given its importance and with the development of instruments and observing techniques, direct imaging has been extensively performed in recent years with large-aperture telescopes. Lafrenière et al. (2007) calculated the planet frequency around a single star as less than 0.1 (for separations in the range 50–250 AU and planet masses 0.5–13 M_J) on the basis of the Gemini observations of 85 stars. In Nielsen & Close (2010), the frequency (8.9–911 AU, $> 4 M_J$) was estimated to be below 0.2, by compiling the data of 118 stars (Liu 2004; Masciadri et al. 2005; Marois et al. 2006; Biller et al. 2007; Lafrenière et al. 2007). Moreover, Chauvin et al. (2010) reported VLT observations of 88 targets (10–500 AU, $> 1 M_J$) that yielded a frequency of below 0.1. Vigan et al. (2012) reported the frequency of a planet around early type stars (A–F) to be $8.7_{-2.8}^{+10.1}$ (1σ). The result of the previous direct imaging surveys for the frequency of a planet summarized in Table 1. The problem with direct imaging is that the sample size is small compared to that of indirect observations.

In these imaging studies, the targets belong to the moving groups and local associations including the β Pictoris moving group, TW Hya Association, Tucana-Horologium Association, and AB Doradus group (Lafrenière et al. 2007; Chauvin et al. 2010). Because these associations are nearby (~ 20 –100 pc) and young (several to several hundred Myr), their planets are relatively bright and should be easy to detect. In addition, stars in the same cluster have similar ages and distances from earth, which statistically improves the accuracy of the age and luminosity estimates, and hence the derivation of the planetary mass. However, the number of the group members is not large. For instance, such sparse moving groups have only several dozen members each, and only a dozen stars have been observed by previous studies (Chauvin et al. 2010). In contrast, open clusters usually have many more members, which can be an advantage when discussing the frequency of planets at specific ages, as well as for obtaining relatively accurate estimates of planetary masses.

We therefore have started an imaging survey of planets in an open cluster, the Pleiades, in order to constrain the frequency of gas-giant planets at >50 AU around the member stars. The imaging is conducted with the near-infrared instrument HiCIAO with the AO188 adaptive optics on the Subaru telescope (Suzuki et al. 2010; Hodapp et al. 2008). Here we report the imaging results for the first 20 surveyed stars.

Table 1. Summary of the direct imaging observations.

Author	Sp. Type (median)	Target cluster *	Age (Myr) (median)	Distance (pc) (median)	Number	Investigated range Mass (M_J)	Separation [†] (AU)	Planet frequency (%)
Lafrenière et al. (2007)	F2–M4 (K0)	1, 2, 3, 5, 8, 9, 10, 11, 14	10–300 (100)	3.2–34.9 (22)	85	0.5–13	50–250 (sma)	≤ 9.3
Chauvin et al. (2010)	B7–M8	2, 3, 4, 5, 6, 7, 12, 14	8–100 ()	10–130 ()	88	0.5–15	10–500 (pro)	< 10
Nielsen & Close (2010)	A5–M5 (K1)	1, 2, 3, 5, 8, 9, 10, 11, 12, 12, 13, 14	2–8800 (160)	3.2–77.0 (24)	118	> 4	8.9–911 (sma)	< 20
Vigan et al. (2012)	A0–F5 (A3)	-	8–400 (100)	19–84 (50)	42	3–14	5–320 (sma)	$8.7^{+10.1}_{-2.8}$

* Moving groups: (1) α Persei; (2) AB Doradus; (3) β Picoris; (4) Carina; (5) Carina-Near; (6) Columba; (7) η Cha; (8) Hercules-Lyra; (9) IC2391; (10) Local association; (11) Local association subgroup B4; (12) Tucana-Horologium; (13) TW Hydrae association; (14) Ursa Major.

[†] Separation: sma: semi-major axis; pro: projected

2. Target selection

Our purpose is to detect extrasolar planets of less than 10 Jovian masses as close as possible to the central star. Therefore, we selected the Pleiades, a nearby young star cluster observable from the northern hemisphere. The Pleiades cluster is significantly populous and thus it provides a better probe of the planet frequency at a given age and for a given common star-formation history. It is located at 133.5 ± 1.2 pc (An et al. 2007; Soderblom et al. 2005; van Leeuwen 2009) and is 125 ± 8 Myr old (Stauffer et al. 1998). The typical metallicity of the cluster members is similar to that of the Sun ($[\text{Fe}/\text{H}] = -0.03 \pm 0.06$; Gratton 2000).

One of the important criteria for choosing an open cluster is the sensitivity for detecting giant planets of $< 10 M_J$. The luminosity of a planet depends on its age and mass. To be consistent with previous studies, in our work, we have adopted the evolutionary model of Baraffe et al. (2003) to predict the brightness of planets. The H -band magnitudes for a planet at 125 Myr are thus estimated to be 27.9, 22.5, and 20.4 magnitudes (mag) for 1, 5, and 10 M_J , respectively. The typical integration time in our observations is about 30 minutes with HiCIAO/AO188, as described later, which provides a detection limit (5σ) of 21.5 mag. This means that it is possible to detect a planet less massive than 10 M_J .

We note that it has been predicted that the formation process itself is also related to the luminosity evolution of a planet. There are two types of evolutionary models: hot start

and cold start. Since the hot-start model assumes higher entropy for giant planets, it may correspond to planet formation by the collapse of a gaseous disk (Baraffe et al. 1998; Baraffe et al. 2002; Baraffe et al. 2003; Chabrier & Baraffe 2000), while the cold start condition may represent core accretion process (Fortney et al. 2005; Fortney et al. 2008; Marley et al. 2007). It has been shown that higher initial entropy causes a planet to become brighter (Spiegel & Burrows 2012). Thus, the brightness of a planet at a certain age as derived by the hot start model serves as an upper limit, while the cold start model represents a lower limit. The model by Baraffe et al. (2003) is a hot start model. Based on the cold start model (Spiegel & Burrows 2012), the H magnitude is predicted to be 22.6 mag for a planet with $12 M_J$, indicating that we do not have the sensitivity to detect such planets. Since planet mass estimates are dependent on the evolutionary model that is used, we should be aware of such uncertainties.

Target stars in the Pleiades were selected on the basis of the following three criteria.

1. The star is brighter than 12 mag in the R band.

AO imaging requires a guide star to measure and correct the atmospheric distortion in optical, so the star should be bright in R to obtain diffraction-limited performance. In the case of Subaru/AO188, the guide star needs to be located within $30''$ of the target; thus, the target star itself is normally used as the AO guide star.

2. The membership probability is high.

Cluster membership for the target star is confirmed by using the following three criteria. First, the membership probability should be higher than 80% based on the proper motion measurements of Belikov et al. (1998) and the target star should not be classified as a non-member by the other proper motion tests of Lodieu et al. (2007). Second, if the star fails to fulfill the first sub-criterion, it needs to have a membership probability (Belikov et al. 1998) higher than 50% and be determined to be a member according to Lodieu et al. (2007). Third, if the star does not satisfy the above two sub-criteria, it should be classified as a Pleiades member on the basis of the proper motion and photometry of Stauffer et al. (2007).

3. The star has no binary companion that might exert gravitational influence on planet formation.

The target star should not be identified as a binary in literature (Bouvier et al. 1997; Raboud & Mermilliod 1998; Lodieu et al. 2007). In addition, there should be no other bright (<15 mag in the H band) object in the field of view (FoV) of $20'' \times 20''$ by 2MASS observation.

Finally, we selected 60 targets out of 455 stars in the Pleiades (Belikov et al. 1998; Micela et al. 1996; Pinfield et al. 2003; Raboud & Mermilliod 1998).

Table 2. Summary of the observations.

Name	Sp. Type	Date	Obs. mode/ Filter	H/K_S [§] (mag)	R (mag)	T_{exp} (sec)	N_{exp}	T_{total} (min)	Ang. FoV (degree)
BD +22 574	F8*	2009-10-31	ADI / H	8.854	10.02	10	207	34.5	116.9
HD 23912	F3V*	2009-10-31	ADI / H	8.097	8.88	10	30	5	4.1
		2010-01-23	ADI / H			10	175	29.2	72.8
		2011-01-27	DI / H			10	30	5	-
V1171 Tau	G8 [†]	2009-11-01	ADI / H	9.270	10.58	10	30	5	28.1
		2012-12-31	DI / H			30	15	7.5	-
HII 2462	G2 [†]	2009-12-22	ADI / H	9.699	10.87	10	60	10	52.8
HD 23863	A7V*	2009-12-23	ADI / H	7.599	7.98	10	93	15.5	46.3
HD 282954	G0 [†]	2010-01-24	ADI / H	8.851	9.98	10	223	37.2	90.9
		2012-09-12	DI / H			2.5	36	1.5	-
HD 23514	G0*	2010-12-01	ADI / H	8.291	8.96	10	204	34	147.6
HD 23247	F3V*	2011-01-27	ADI / H	7.811	8.85	10	83	13.8	79.7
		2011-12-23	ADI / H			10	65	10.8	-
V855 Tau	F8 [†]	2011-01-28	ADI / H	8.337	9.37	10	160	26.7	114.8
		2012-01-01	DI / H			10	270	45	-
HD 24132	F2V*	2011-01-29	ADI / H	7.930	8.59	10	134	22.3	107.9
HD 23061	F5V*	2011-01-30	ADI / H	8.325	9.28	10	149	24.8	103.5
TYC 1800-2144-1	G0V [†]	2011-01-31	ADI / K_S	8.868	10.37	10	58	9.7	72.5
HII 1348	K5 [†]	2011-12-23	ADI / H	9.831	11.92	10	141	23.5	90.4
Melotte 22 SSHJ G214	G2 [†]	2011-12-23	ADI / H	9.634	11.17	10	180	30	59.1
BD +23 514	G5 [†]	2011-12-24	ADI / H	9.528	10.90	10	121	20.2	97.3
Melotte 22 SSHJ G213	G2 [†]	2011-12-24	ADI / H	9.543	10.91	5	410	34.2	31.4
Melotte 22 SSHJ G221	G2IV [‡]	2011-12-25	ADI / H	9.311	10.76	10	270	45	41.9
V1054 Tau	-	2011-12-30	ADI / H	9.921	11.35	10	150	25.8	105.2
V1174 Tau	-	2011-12-30	ADI / H	10.197	11.61	10	170	28.3	21.3
Melotte 22 SSHJ K101	-	2011-12-31	ADI / H	9.959	11.69	10	80	13.3	58.4

DI; direct imaging. ADI; angular differential imaging. T_{exp} ; integration time of each exposure. N_{exp} ; total number of exposures. T_{total} ; total exposure time. Ang. FoV; rotation angle of field of view during observation.

* Wright et al. 2003

† Skiff 2010

‡ Belikov et al. 2002

§ Hmag; Cutri et al. 2003, Rmag; Zacharias et al. 2005

3. Observations

Twenty of the 60 selected target stars were observed between October 2009 and January 2012 (Table 2). The imaging observations were carried out as part of the Strategic Explorations of Exoplanets and Disks with Subaru (SEEDS, Tamura 2009) by using HiCIAO, which is a high-contrast instrument installed on the Subaru telescope (Suzuki et al. 2010; Hodapp et al. 2008). HiCIAO has a 2048×2048 HgCdTe/HAWAII 2 detector array and its pixel scale is 9.5 mas/pixel; thus, the FoV is $\sim 20'' \times 20''$. The targets were observed either with the H or K_S filter. The coronagraphic masks were not used.

To obtain the high contrast needed to observe within the close vicinity of a host star, HiCIAO was used in combination with AO188 (Hayano et al. 2010). By using AO, a FWHM of 6–10 pixels ($0''.05$ – $0''.10$) was achieved for a point source. In addition, angular differential imaging (ADI; Marois et al. 2006) was implemented. ADI is an imaging method that allows the rotation of the FoV with time but fixes the detector plane relative to the pupil plane by using an image-rotator. As a result, this method can effectively reduce quasi-static noise including the halo of the star and speckles produced by the telescope, because the noise pattern is fixed on the detector. The key to obtaining effective noise reduction is a large field rotation; therefore, the imaging was performed to cover the period of transit of the target stars over the meridian, giving a rotation angle of 25–150 degrees. Additionally, the target star was placed at the center of the FoV to provide a wide area for the planet search.

Our observational procedure consisted of three steps. First, 5–10 unsaturated frames were taken as a reference for the point-spread-function (PSF) of the central star with 1.5 to 2.5 s exposure time to avoid saturation. Second, the ADI observations were performed over an integration of 5 or 10 s in the individual frames to obtain high sensitivity, but with no smearing caused by the field rotation. The central star was saturated at the peak by this integration time, and the saturated area had a radius of 3–6 pixels. Third, several unsaturated frames were retaken. Table 2 summarizes the information on the observed stars, observing mode, filters, and exposure times of saturated images.

If sources were detected around a target star, they were considered to be candidate companions (CCs). For HD 23247, the bright ($H < 14.5$) companion candidate was detected at $3''.7$ from the central star. However, we discuss only CCs fainter than 14.5 mag which corresponds to about $100 M_J$ (brown dwarf mass), in the subsequent part of this paper since our focus is not on the stellar regime. The relative positions of CCs against the target star were measured in the follow-up observations for HD 23912 and V855 Tau to determine whether they were co-moving. In the follow-up observations, the direct imaging (DI) mode without field rotation was employed since the CCs have wide angular separation (more than about 3 arcsec). V1171 Tau, BD+22 574, and HD 282954 have been observed with a different camera, Subaru/CIAO, in 2005, and the same CCs were detected (Itoh et al. 2011). Thus, our HiCIAO

observations gave the proper motion measurements combined with the CIAO results. HD 23912 was observed three times (in October 2009, January 2010, and January 2011). Since the field rotation by ADI was too small (~ 10 degree) for the first imaging in October 2009, it was revisited in January 2010.

4. Data reduction

The first step of the image processing was to remove the striped pattern caused by fluctuations in the bias levels in the individual raw images. The stripes consist of two components: 32 horizontal stripes each with a height of 64 pixels, and thin vertical stripes, each 2048 pixels high, randomly distributed over the image. These patterns vary with time and are independent among images. We created the striped pattern for the whole FoV by using the sky region in each frame, and subtracting it from the raw frame, a process corresponding to sky subtraction. Next, the bad pixels and their clusters were corrected by subtracting the de-striped dark image. Then, we performed flat-fielding by using the dome-flats. Bad pixels randomly occurring in arbitrary pixel positions were interpolated from the surrounding pixels. These calibrations were carried out by using our own reduction tool for HiCIAO data.

The image processing that follows (described below) was performed with IRAF¹. Sub-pixel shifts cannot be avoided during the process of distortion correction and ADI reductions. They require the interpolation of adjacent pixels, which causes the smearing of pixel values. As a result, the noise level is reduced. Moreover, the amount of sub-pixel shift was different for each frame, and we confirmed that the degree of noise reduction could vary among multiple images. Such a non-uniform process, as well as artificial noise reduction, may affect our discussion of detection limits. Thus, before applying the distortion correction, all images were smoothed with a 2-D Gaussian filter with an FWHM of 3 pixels to obtain the same level of noise reduction for all pixels and images. The distortion was measured by comparison of images of the globular clusters (M5 and M15) with HiCIAO and HST/STIS (van der Marel et al. 2002). The distortion was then corrected to obtain a pixel scale of 9.500 ± 0.005 mas/pixel. The precision of the distortion correction is as described below.

Next, in preparation for the ADI reductions, the stellar position was measured and matched to the image center for all the frames. The target stars were saturated in areas of 3–6 pixels in radius. For removal of the stellar halo by ADI reductions, we adopted the centroid position of the halo measured from 10 to 50 pixels in radius as the stellar position. For the ADI processing, we followed the standard ADI procedures described by Marois et al. (2006). First, a reference image was created by calculating the median at each pixel position using all images. Second, the reference was subtracted from the individual frames. The resultant image

¹ IRAF is distributed by the National Optical Astronomy Observatories, which are operated by the Association of Universities for Research in Astronomy, Inc., under cooperative agreement with the National Science Foundation.

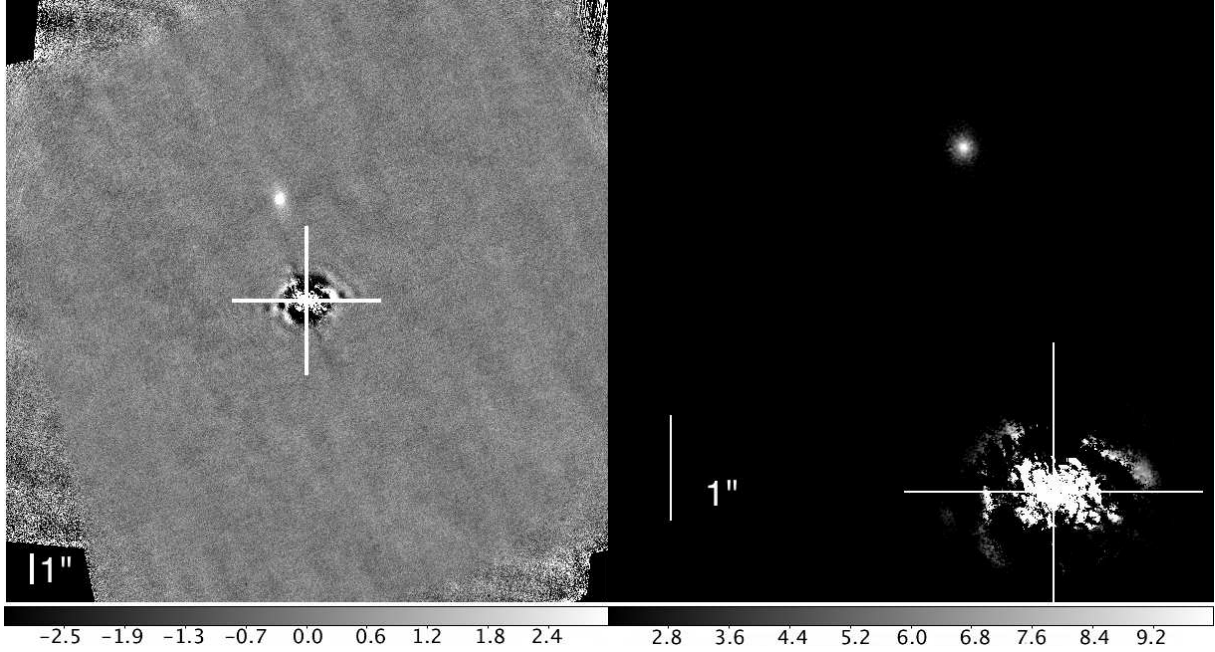


Fig. 1. The result of ADI reductions for HD 23912. The image was obtained in the H band. The white cross indicates the position of the central star. A point source was detected at an angular separation of $3''38$. North is on the top and east is to the left. *Left panel:* The field of view is $19''5 \times 19''5$. The pixel value range is -0.4 to $+0.6$ ADU. The four corners cannot be discussed since these regions are outside the FoV in many frames. *Right panel:* The zoom-in image of the companion candidate. The field of view is $5''8 \times 5''8$. The pixel value range is $+0.0$ to $+5.0$ ADU.

was de-rotated to align the field so that north was on the top. Finally, the de-rotated images were median-combined with 5σ clipping to obtain enough sensitivity to detect planetary-mass objects.

An example of the final reduced image is presented in Figure 1. The image was obtained using data from HD 23912 in the H band taken in January 2010. The rotation angle of the FoV was 73 degrees and the total integration time was 29.2 minutes. At the center of the left image, the residual pattern of the subtraction of the stellar halo can be seen. A point source is detected at $3''388 \pm 0''028$ from the star with a position angle (P.A.) of $14^\circ 92' \pm 0^\circ 48'$. During the ADI, more images are taken at similar P.A. of the field when the rotation is slow. The emission from point sources in such images cannot be completely eliminated in the reference image, and consequently, self-subtraction occurs in the faint outskirts of the point source. This is consistent with the sculpting along the azimuthal direction. Images of all the target stars are shown in the Appendix.

When a CC was detected, the relative position between the CC and the central star was measured. The centroid position of the CC was determined using an aperture with radius of 1 FWHM. A position measurement was performed in each frame or combined frame depending on the brightness of the CC. In order to determine the position of the central star in saturated

images, we first, in unsaturated images, determine the offset between the center derived by Gaussian fitting and a centroiding algorithm with a mask equal in size to the saturated area in saturated images. Assuming the same offset holds true in the saturated case, we correct the measurement derived by this masked centroiding algorithm accordingly. The uncertainty of the position measurement was checked by the deviation from the rotation center of the field by ADI. The relative positions were measured in each (combined) image, and the rotation center was defined as the center of the fitted circular orbit for the CC in multiple images without de-rotation. Moreover, the deviation between the position of the CC and its fitted circular path due to the ADI observation was below 0.7 pixels. This deviation encompasses possible distortions left even after distortion correction (as the shape would not be perfectly circular), thus showing that as far as any measurable effect exists it is small. The results of the astrometry measurements are summarized in Table 3.

The magnitude of the CCs was estimated by the target star as the flux calibrator. The magnitudes of both for the central stars and the CCs were measured by aperture photometry. For the central star, photometry was performed by using the unsaturated frames taken before and after the ADI observations as mentioned in section 3. The background level was estimated as the centroid of the pixel-values histogram in an annulus with a radius of 50 pixels and the width of 20 pixels. The aperture size varied from 2 to 40 pixels in radius, and the converged magnitude, at a radius of about 20 pixels depending on the targets, was taken to be its magnitudes. By comparing this instrumental magnitude with the 2MASS measurement under the assumption that the star was not variable, the conversion from ADU to magnitude was obtained. The photometry for the CCs was performed with the same aperture size as that for the central star. The flux loss by the image processing including the ADI reductions was $\sim 5\%$, estimated by embedding an artificial point source at radially equally spaced angles and distances (interval of $1''$) in the raw image and applying the same reduction procedures. The flux loss was independent of the separation beyond $1''$. The photometry result obtained for the CCs was corrected for this flux loss. Finally, the magnitude of the CCs was calculated using the conversion from ADU to the magnitude derived from the photometry of the central star. To improve the signal-to-noise ratio (S/N), the photometry for a CC was performed with images in which 20–40 frames were combined and the results were averaged. The H magnitudes for the CCs are shown in Table 3.

5. Results

5.1. Detection limits of our observations

The detection limit of our observations is defined by a signal-to-noise ratio (S/N) of 5. The noise was determined by the standard deviation of the background level in the azimuthal direction measured at the same distance from the target star. The background level was

Table 3. Astrometry and photometry of companion candidates.

Name	Separation Angle (")	P.A. (° E of N)	H (mag)	Mass* (M_J)	UT Date	Status
V1171 Tau CC1	12.770 ± 0.025	135.50 ± 0.40	18.3^\dagger	-	2005-11-17 [‡]	-
	12.629 ± 0.028	134.75 ± 0.10	17.8 ± 0.1	22	2009-11-01	-
	12.603 ± 0.031	134.08 ± 0.21	17.8 ± 0.3	22	2012-12-31	B
V1171 Tau CC2	12.880 ± 0.027	136.77 ± 0.40	18.3^\dagger	-	2005-11-17 [‡]	-
	12.744 ± 0.020	136.15 ± 0.10	18.5 ± 0.6	19	2009-11-01	-
	12.628 ± 0.031	135.51 ± 0.21	18.5 ± 0.6	19	2012-12-31	B
HD 23912 CC1	3.388 ± 0.028	14.92 ± 0.48	17.4 ± 0.1	26	2010-01-23	-
	3.435 ± 0.008	14.52 ± 0.28	17.2 ± 0.2	28	2011-01-27	B
BD +22 574 CC1	3.405 ± 0.025	95.70 ± 0.20	$-\S$	-	2005-11-17	-
	3.288 ± 0.033	92.57 ± 0.20	19.2 ± 0.2	13	2009-10-31	Probably B.
BD +22 574 CC2	8.440 ± 0.030	51.82 ± 0.10	18.6^\parallel	14	2005-11-17	-
	8.501 ± 0.033	50.01 ± 0.10	17.4 ± 0.2	26	2009-10-31	U
HD 282954 CC1	9.006 ± 0.030	103.82 ± 0.50	16.4^\parallel	33	2005-11-17	-
	9.031 ± 0.014	103.23 ± 0.18	14.6 ± 0.1	87	2010-01-23	-
	8.943 ± 0.014	103.28 ± 0.20	14.4 ± 0.2	99	2012-09-12	B
V855 Tau CC1	8.05 ± 0.03	19.46 ± 0.21	17.2 ± 0.4	27	2011-01-28	-
	-	-	-	-	2012-01-01 [#]	?
HD23514 CC1	2.64 ± 0.02	228.7 ± 1.0	-	-	2006-12-10 ^{**}	-
	2.64 ± 0.01	227.8 ± 0.3	-	-	2007-10-25 ^{**}	-
	2.62 ± 0.04	227.2 ± 0.5	-	-	2008-11-04 ^{**}	-
	2.642 ± 0.040	227.51 ± 0.04	15.61 ± 0.08	52	2009-11-01 ^{**}	-
	2.644 ± 0.002	227.48 ± 0.05	15.39 ± 0.06	58	2010-10-30 ^{**}	-
	2.646 ± 0.033	227.59 ± 0.72	15.37 ± 0.05	58	2010-12-01	C
HII 1348 CC1	1.09 ± 0.02	347.9 ± 0.7	-	-	1996-09-25 - 10-01 ^{††}	-
	1.097 ± 0.005	346.8 ± 0.2	15.30 ± 0.09	60	2004-10-03 ^{‡‡}	-
	1.12 ± 0.02	346.8 ± 0.6	-	-	2005-11-21 ^{§§}	-
	1.12 ± 0.03	346.1 ± 0.9	15.7 ± 0.4	48	2011-12-23	C
V1054 Tau CC1	7.110 ± 0.014	110.29 ± 0.11	18.1 ± 0.4	20	2011-12-30	N
V1054 Tau CC2	7.361 ± 0.028	76.48 ± 0.22	15.97 ± 0.09	44	2011-12-30	N
V1174 Tau CC1	6.473 ± 0.033	63.68 ± 0.28	18.0 ± 0.4	21	2011-12-30	N
V1174 Tau CC2	9.24 ± 0.03	37.4 ± 0.2	18.5 ± 0.3	17	2011-12-30	N

Much brighter companion candidate was detected within $3.7''$ arcsec for HD 23247. However, only candidates less massive than the brown-dwarf mass ($\sim 100 M_J$) are discussed in this paper.

Status sign; U presents "undefined" due to the uncertainty of the proper motion measurement. B presents the background object. C presents the co-moving object. N presents that the proper motion has not been measured yet.

* The masses are linearly interpolated by reference to Baraffe et al. (2003). [†] It was impossible to measure the individual brightness of CC1 and CC2, because they were not spatially separated not well enough for aperture photometry. In addition, the error was difficult to determine due to the fluctuated PSF because of the poor seeing. [‡] Subaru/CIAO, Subaru/IRCS (Itoh et al. 2011). [§] It was impossible to measure the brightness of the CC due to the stellar halo. ^{||} K magnitude. It was impossible to estimate the error due to the variation of PSF because of the inclement weather. [#] The companion

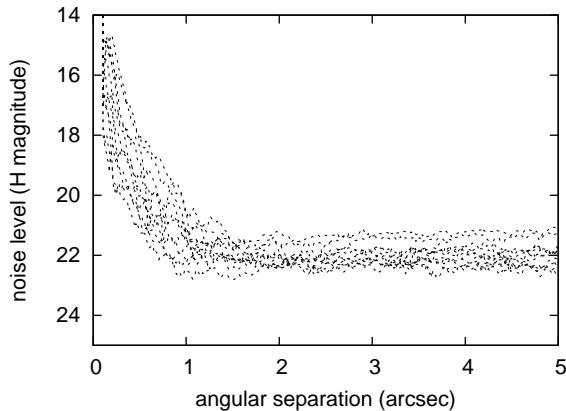


Fig. 2. Noise level (1σ) as a function of angular separation. Dotted lines indicate individual observations obtained from October 2009 to January 2012. The total integration time in each observation is in the range of 5–45 minutes.

obtained with an aperture size of approximately $2 \times \text{FWHM}$ on the median-combined image by ADI reductions. The relation between the standard deviation ($S/N=1$) and angular separation from the central star is plotted in Figure 2. The median of the detection limits for all ADI observations becomes constant at 20.8 mag for S/N of 3 and 20.3 mag for S/N of 5 in the region beyond $1''.5$ from the central star. Inside $\sim 1''.5$, the detection limit is determined by the subtraction residual of the stellar halo. It is 17.7 mag and 19.7 mag for separations of $0''.5$ and $1''.0$, respectively.

We note that there are other ways to achieve better suppression of the stellar halo than the classical ADI reductions, such as Locally Optimized Combination of Images (LOCI: Lafrenière et al. 2007). The LOCI algorithm considers spatial correlations of the stellar halo and speckle noise with reference images. However, our primary focus in this paper is on the relatively distant region from the star (more than about 100 AU) where uncorrelated, random noise is dominant and classical ADI is more effective than LOCI. The results of standard ADI reductions are thus discussed in this work.

5.2. Astrometry and photometry of companion candidates

Among 13 companion candidates, a CC for HD 23912 is detected in our follow-up imaging with HiCIAO while the CC of V855 Tau is not found in the follow-up. Another 7 CCs around 5 stars (BD+22 574, V1171 Tau, HD 282954, HD 23514, and HII 1348) were observed with Subaru/CIAO, Subaru/IRCS, Keck/NIRC2, CFHT/PUEO, Palomar Hale telescope/PHARO, Keck/OSIRIS at the previous epochs (Itoh et al. 2011; Rodriguez et al. 2012; Bouvier et al. 1997; Geißler et al. 2012). The relative distances to the central stars for these CCs are shown in Figure 3. The remaining 4 CCs, 2 for V1054 Tau and V1174 Tau respectively, are waiting for the second epoch observations for proper motion measurements.

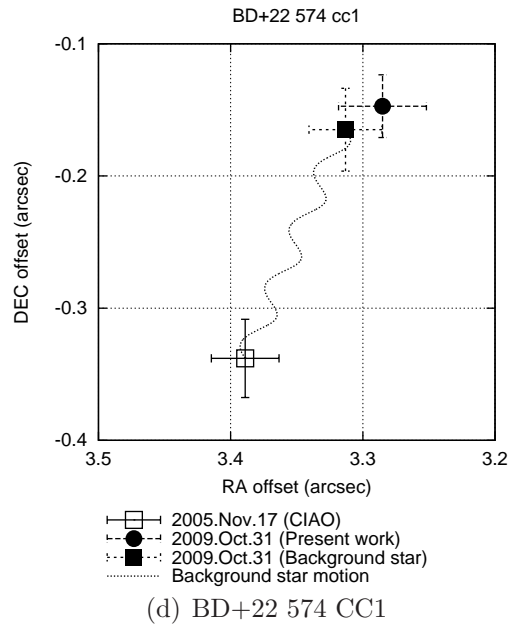
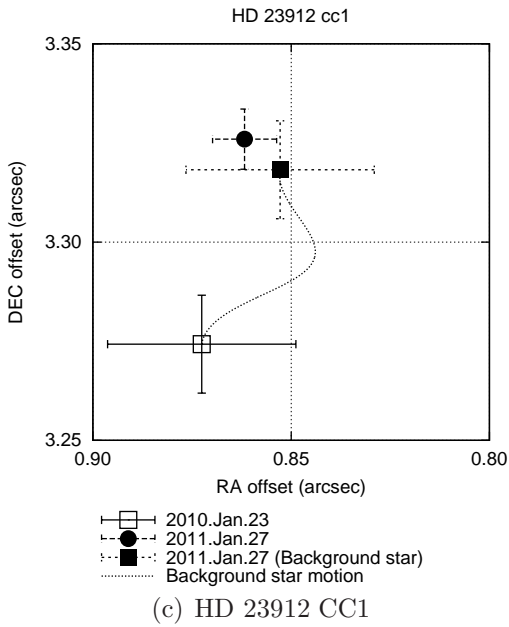
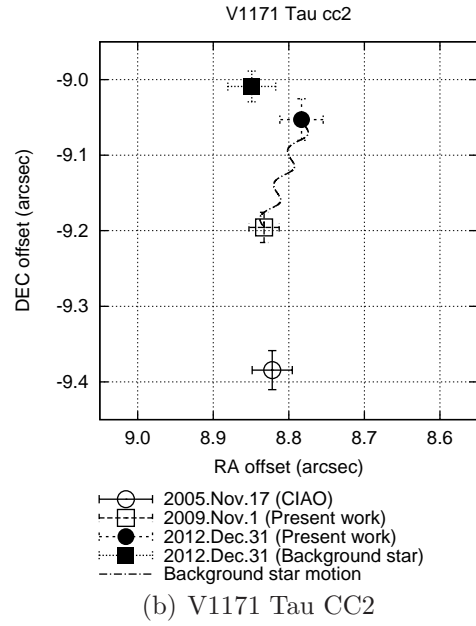
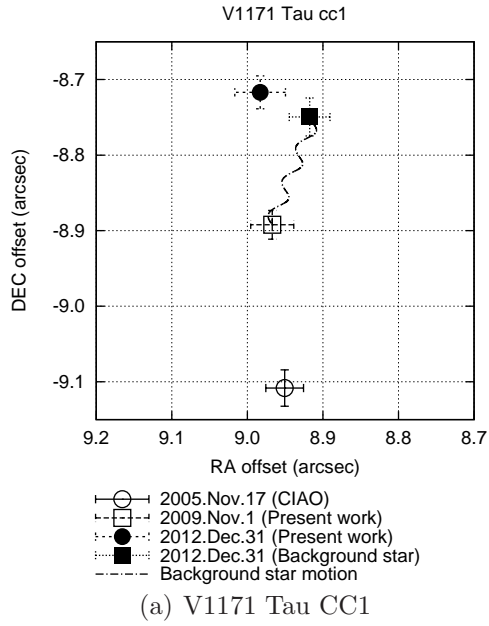
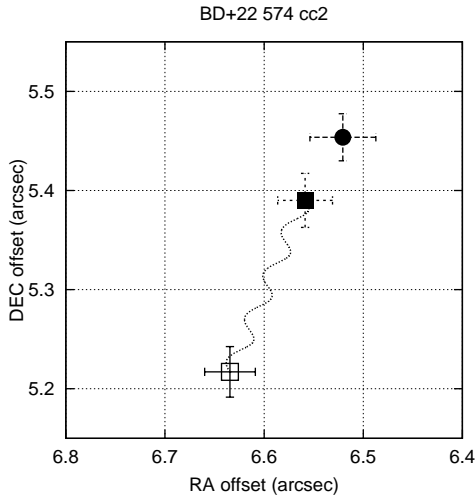
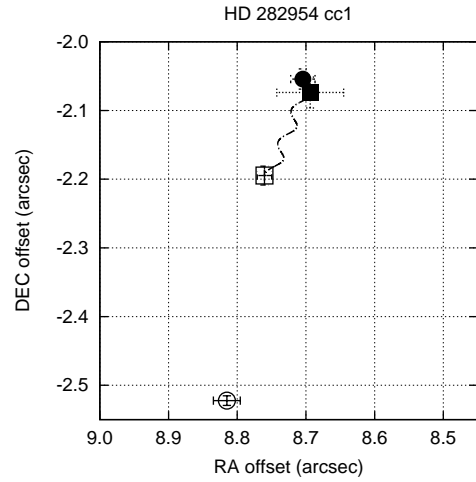


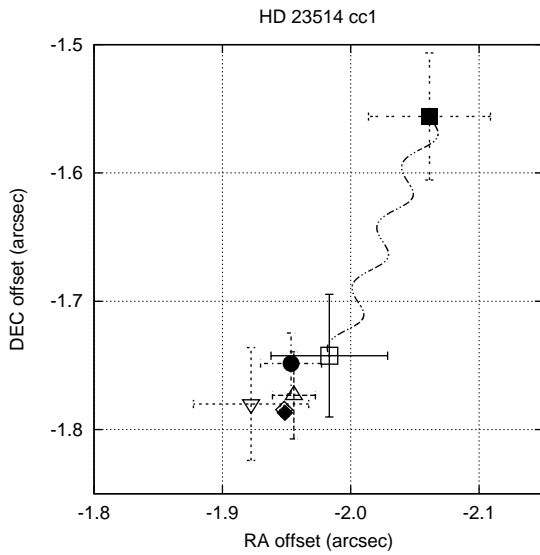
Fig. 3. Top left panel: V1171 Tau CC1. Top right panel: V1171 Tau CC2. Lower left panel: HD 23912 CC1. Lower right panel: BD +22 574 CC1.



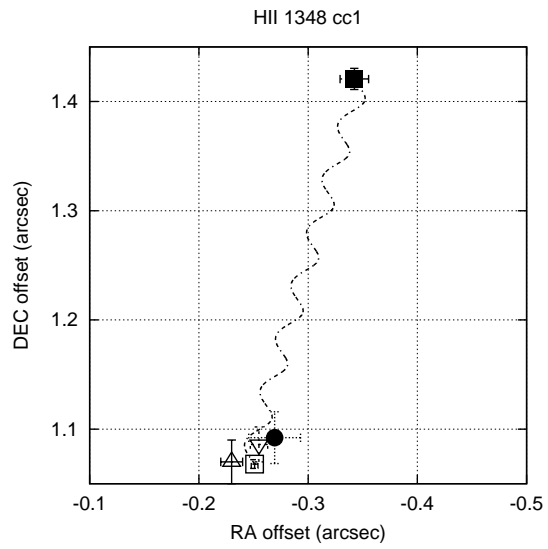
(e) BD+22 574 CC2



(f) HD 282954 CC1



(g) HD 23514 CC1



(h) HII 1348 CC1

Fig. 3. *Continued.* Top left panel: BD +22 574 CC2. Top right panel: HD 282954 CC1. Lower left panel: HD 23514 CC1. Lower right panel: HII 1348 CC1.

5.2.1. *HD 23514, and HII 1348*

HD 23514 and HII 1348 have a co-moving object respectively, which is most likely a companion gravitationally bound to it (Figure 3(g), and Figure 3(h)). The companion objects were first identified by the previous astrometry by Rodriguez et al. (2012) for HD 23514, and by Geißler et al. (2012) for HII 1348. The H magnitudes for the companion were measured to be 15.39 ± 0.06 mag in October 2010 for HD 23514, and 15.30 ± 0.09 mag in October 2004 for HII 1348, and their masses are estimated as $60 M_J$, which is in the brown dwarf regime.

Rodriguez et al. (2012) measured the separation and the P.A. of HD 23514 as $2''642 \pm 0''003$ and $227^\circ51 \pm 0^\circ04$ in November 2009, and in October 2010 they were $2''644 \pm 0''002$ and $227^\circ48 \pm 0^\circ05$, respectively. In our observation in December 2010, the separation was $2''646 \pm 0''033$ and the P.A. was $227^\circ6 \pm 0^\circ7$. The H magnitude of the CC in December 2010 was 15.37 ± 0.05 . Our measurements are therefore consistent with those of Rodriguez et al. (2012).

For the companion of HII 1348, Geißler et al. (2012) measured the separation and the P.A. as $1''097 \pm 0''005$ and $346^\circ8 \pm 0^\circ2$ in October 2004, and in November 2005 they were $1''12 \pm 0''02$ and $346^\circ8 \pm 0^\circ6$, respectively. In our observation in December 2011, the separation was $1''12 \pm 0''03$ and the P.A. was $346^\circ1 \pm 0^\circ9$. The H magnitude of the CC in December 2011 was 15.7 ± 0.4 . Our measurements are therefore consistent with those of Geißler et al. (2012).

5.2.2. *V1171 Tau, HD 282954 and BD+22 574*

We observed HD 282954 and V1171 Tau two times for measurement of their proper motions with HiCIAO. We confirmed these 3 CCs were the background stars from comparison of the astrometry between the two epochs. Two CCs for BD+22 574 show changes in their relative distances to the central star between the two epochs, and are likely to be background stars. We consider it likely that the distortion correction is not perfect for the CIAO data because the distortion map for the CIAO data cannot be properly generated due to a limited number of the field stars in Trapezium, which was observed for the distortion correction. However, because the distortion is small at narrow separation, the CC1 of BD+22 574 (separation $\sim 3''3$) is confirmed as the background star. It is not clear whether BD+22 574 CC2 is the companion or the background star.

5.2.3. *V855 Tau, and HD 23912*

One CC was detected for V855 Tau in January 2011. Interestingly, however, it was not detected in January 2012. It is difficult to conclude that we had a false detection in 2011 because it is not one of the known artifacts, it is seen in all of the several combined images, and its PSF has a reasonable FWHM without any peculiarity in its shape. It may therefore be a foreground object. HD 23912 also has one CC, but it turned out to be a background star on the basis of ADI and DI observations with HiCIAO.

5.3. Statistical analysis for estimating the frequency of planets

The purpose of this subsection is to constrain the frequency of planets around a star based on our observations. First, we define and calculate the detection efficiency ε_n as the probability of planet detection when host star n has one gas-giant planet.

To begin with, we consider the separation range where we can detect a planet in our observations with HiCIAO/AO188. The detection limit of a point source far from the central star is determined solely by the total integration time without being affected by the stellar halo. As already mentioned in section 5.1, the detection limit of our observations (5σ) was 20.3 magnitudes with an integration time of 5–45 minutes beyond $1''.5$. However, residuals of the stellar halo remain in the inner ($<1''.5$) region as seen in Figure 2. In this area, only brighter planets, brown dwarfs, and stars can be detected, but we are interested in the region where planets can be detected if they exist. The minimum separation for planet detection, which we define as the inner working angle (IWA), can depend not only on the sensitivity but also on the field rotation of ADI. In this way, the IWA is determined only by the sensitivity of our observations, which is $0''.6$ – $1''.0$ arcsec, depending on the amount of suppression of the stellar halo for each target. Nevertheless, most of the region we consider below is the outer part ($>1''.5$), which is free from the effect of the stellar halo. In the following calculation, F_{\min} is defined as the minimum angular separation that a planet with a given mass M_P can be detected.

The H magnitude can be converted to planetary mass by using the evolutionary model by Baraffe et al. (2003), assuming an age of 125 Myr and a distance of 135 pc for the Pleiades. Using this relation, the minimum detectable planet mass M_{\min} can be determined for each separation.

Next, we calculate the detection efficiency, which is the probability that planets lie in the detectable parameter space of the observation. The detection efficiency $\varepsilon(M_P, a, e)$ to find a planet with a certain orbit in the Pleiades is derived from the planet mass M_P , semi-major axis a , and eccentricity e . Here, we assume that a host star always has one planet that has the orbital elements; a , e , inclination i (angle between line of sight and normal to the orbital plane), and azimuth ϕ (angle between line of sight and periapsis). As the planet moves along its orbit, the separation angle F from the central star to the planet varies with the true anomaly θ as described as follows:

$$F = \frac{a(1 - e^2)}{D(1 + e \cos \theta)} \sqrt{\cos^2(\theta - \phi) \cos^2 i + \sin^2(\theta - \phi)}, \quad (1)$$

where D is the distance to the Pleiades cluster ($D = 135$ pc). We then introduce T_d , which is the time per orbital period T_P for a planet of M_P being in the range of $F \geq F_{\min}$. Using T_d , the detection efficiency of a certain orbit is described as $g(M_P, a, e, i, \phi) = T_d/T_P$. Considering that the line of sight is randomly distributed and independent of a planet orbit the detection efficiency for one orbit is

$$\varepsilon(M_P, a, e) = \frac{\int_{i=-\pi/2}^{\pi/2} \sin i \int_{\phi=0}^{2\pi} g(M_P, a, e, i, \phi) d\phi di}{\int_{i=-\pi/2}^{\pi/2} \sin i \int_{\phi=0}^{2\pi} d\phi di}. \quad (2)$$

Accordingly, the detection efficiency ε_n for a host star n can be obtained from the distribution of planet mass, semi-major axis, and eccentricity by

$$\varepsilon_n = \frac{\int_{M_{\min}}^{M_{\max}} \frac{dN}{dM_P} \int_{a_{\min}}^{a_{\max}} \frac{dN}{da} \int_0^1 \frac{dN}{de} \varepsilon(M_P, a, e) dM_P da de}{\int_{M_{\min}}^{M_{\max}} \frac{dN}{dM_P} \int_{a_{\min}}^{a_{\max}} \frac{dN}{da} \int_0^1 \frac{dN}{de} dM_P da de}. \quad (3)$$

Here, we need to consider the number distribution of planet mass, semi-major axis, and eccentricity, which are expressed as dN/dM_P , dN/da and dN/de , respectively. The distribution of planet mass was derived as $dN/dM_P \propto M_P^{-1.2 \sim -1.9}$ by the RV survey for planets with orbital periods longer than 100 days (Cumming et al. 2008). For the distribution of the semi-major axis, $dN/da \propto a^{-0.61}$ was obtained from the RV survey for planets with long orbital periods (shorter than 2000 days: Cumming et al. 2008). Finally, the distribution of eccentricity was derived as $dN/de \propto \exp(-4.2e)$ on the basis of data in The Extrasolar Planet Encyclopedia². We assume these distributions in our calculation.

Adopting Baraffe et al. (2003), the minimum detectable mass in our observation was 6–10 M_J at separations larger than 1".5. As shown in Figure 2, IWAs are 100 AU for a circular orbit and 50 AU for an eccentric orbit with an eccentricity of 0.9, respectively. Considering this result and using equation (3), the detection efficiency ε_n ranges from 82–96% for a planet mass of 6–12 M_J and semi-major axis of 50–1000 AU.

In the above discussion, we calculated the detection efficiency for one planet orbiting one star, ε_n . In the next step, we consider the probability of detecting *at least* one planet, p_n , around a star n ($n = 1 \dots N$). p_n is calculated from the detection efficiency ε_n and the number frequency of planets around a host star η , since

$$p_n = \eta \times \varepsilon_n. \quad (4)$$

As noted above, ε_n is uniquely determined by the orbital distribution of a planet and the detection separation range in the observations. On the other hand, p_n can be constrained by our imaging results for 20 stars. Therefore, it is possible to constrain the planet frequency η for a host star.

In the following analytical approach, we employ Bayes' theorem as described by Vigan et al. (2012) and Lafrenière et al. (2007). The probability of detecting at least one planet is $\eta \times \varepsilon_n$ while that of non-detection is $(1 - \eta \times \varepsilon_n)$. The likelihood of the data given ε_n is described as

$$L(\{d_n\}|\eta) = \prod_{n=1}^N (1 - \eta \varepsilon_n)^{1-d_n} \cdot (\eta \varepsilon_n)^{d_n}, \quad (5)$$

where d_n is the sign of detection, which equals 1 if at least one planet is detected around a

² <http://exoplanet.eu/>

star n and 0 if no planet is detected. On the left-hand side of the equation, $\{d_n\}$ shows the set of results from N observations. Using this likelihood, the conditional probability distribution that the set of events $\{d_n\}$ occurs with frequency η is

$$p(\eta|\{d_n\}) = \frac{L(\{d_n\}|\eta)p(\eta)}{\int_0^1 L(\{d_n\}|\eta)p(\eta)d\eta}, \quad (6)$$

where $p(\eta)$ is the prior probability of η . Since η is unknown a priori, $p(\eta) = 1$.

We can determine the range of η as a confidence interval (CI) on a given confidence level (CL) α ,

$$\alpha = \int_{\eta_{\min}}^{\eta_{\max}} p(\eta|\{d_n\}) d\eta, \quad (7)$$

where η_{\max} and η_{\min} are the maximum and minimum values of η in the case of $\{d_n\}$.

In our observations, there are 8 companion candidates without proper motion measurements (V1171 Tau CC1, CC2, BD+22 574 CC2, HD 282954 CC1, V1054 Tau CC1, CC2, V1174 Tau CC1, and CC2). Even if they are companion objects, their masses are larger than that of planets ($> 12M_J$). Thus, no planets is found around 20 stars in our observations, resulting in a value of η_{\max} of about 17.9% (CL = 95%) for planets in the mass range of 6–12 M_J and the semi-major axis of 50–1000 AU. The minimum value η_{\min} is always 0 in this case.

6. Discussion

On the basis of our observations of 20 stars, the frequency of planets in the mass range of 6–12 M_J orbiting at a distance of 50–1000 AU from a host star in the Pleiades (125 Myr, 135 pc) is estimated to be 17.9% as an upper limit (2σ). This is the first time this constraint has been obtained for a certain age (~ 125 Myr).

In a previous direct imaging survey by Lafrenière et al. (2007), the frequency of planets over the mass and separation ranges of 0.5–13 M_J and 50–250 AU was below 10%, as derived from observations of 85 stars with the Gemini North telescope. Similarly, the frequency of planets of $> 1 M_J$ at 40–500 AU was not greater than 9.3% (2σ) by the VLT observations of 88 stars within 100 pc (Chauvin et al. 2010). Therefore, our estimate is consistent with these previous results, indicating that the planet frequency in the Pleiades is not much higher than in other moving groups and around field stars.

According to these results, giant planets are very rare at larger separations (more than about 50 AU), although there are a few known candidate systems (e.g., Marois et al. 2008; Itoh et al. 2005). Since current formation theory predicts that heavy giant planets can form only via disk instability at distant regions, it is speculated that such instability is not a major in-situ formation process for giant planets. Furthermore, our observations cover a wide area even beyond a few 100 AU which is the typical size of protoplanetary disks (Andrews & Williams 2007), thus it is difficult to expect that planets form in situ at such a distances from a host star. However, it has been suggested that giant planets or their natal fragments in multiple

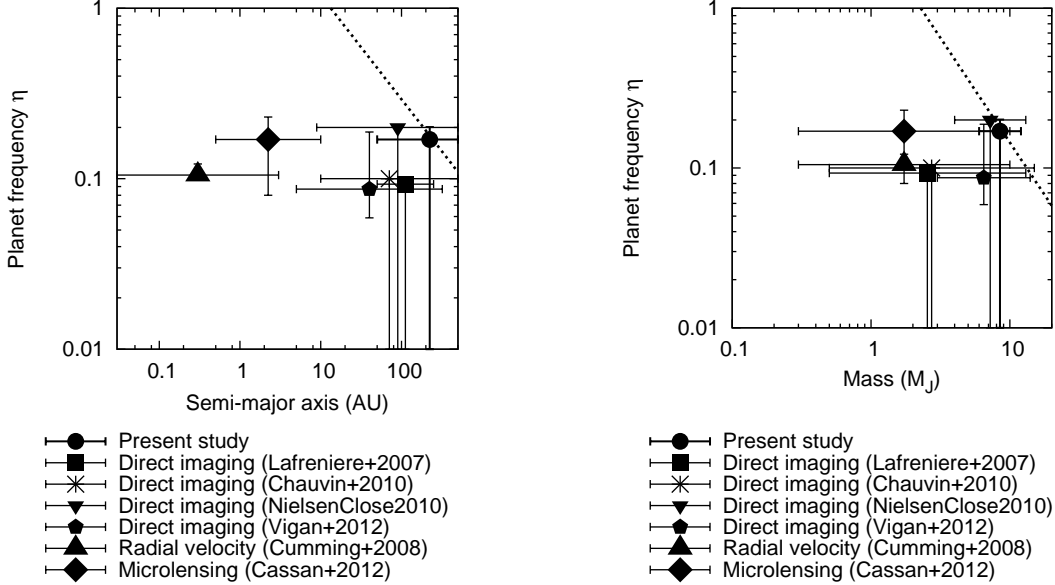


Fig. 4. Planet frequency η as a function of semi-major axis (*left panel*) and planet mass (*right panel*). The *circle* shows our work (50–1000 AU, 6–12 M_J), while the *square* indicates the direct imaging (50–250 AU, 0.5–13 M_J ; Lafrenière et al. 2007). The *rice symbol*, the *triangle* and the *pentagon* shows other direct imaging (10–500 AU, 0.5–15 M_J ; Chauvin et al. 2010), (8.9–911 AU, $>4 M_J$; Nielsen & Close 2010) and (5–320 AU, 3–14 M_J ; Vigan et al. 2012), respectively. The *triangle* denotes the radial velocity (0.03–3 AU, 0.3–10 M_J ; Cumming et al. 2008), and the *diamond* shows microlensing (0.5–10 AU, 0.3–10 M_J ; Cassan et al. 2012). The dotted lines in the two panels indicate the distribution of the frequency of planets that is derived from our observations. The slopes of the lines are -1.31 and -0.61 in the *left* and *right* panels, respectively.

planetary systems can be ejected into very wide orbits (10^2 – 10^5 AU) through gravitational interaction (Basu & Vorobyov 2012; Veras et al. 2009). At present, the observed rareness is not inconsistent with theoretical predictions that invoke planet–planet scattering.

In other planet surveys of the region near host stars using microlensing (OGLE: Beaulieu et al. 2006; Kubas et al. 2008, MOA: Sumi et al. 2010), the frequency of planets with 0.3–10 M_J at 0.5–10 AU was $17^{+6}_{-9}\%$ (Cassan et al. 2012). In addition, the frequency of planets more massive than 0.3–10 M_J over 0.03–3 AU was $10.5 \pm 1.7\%$ by RV survey (Cumming et al. 2008). Though the detectable separation in these other surveys was different from that in direct imaging, the frequency of planets according to our survey does not seem to be higher than those obtained by microlensing and RV surveys (Figure 4, Table 4).

In our observations, point sources fainter than 14.5 mag are detected around 9 of 20 (40%) target stars whether or not they are real companion objects. The detection limit is 20.3 mag in the H band at the separation of $1''.5$ – $10''$. This possibility of finding other point sources is consistent with previous direct imaging studies with similar survey depth and size of the field of view. For instance, CCs were detected toward 32 stars (44%) in the galactic latitude

Table 4. Comparison of observations for planet frequency.

Observation method	Ref.	Distribution index		Planet frequency (η)
		Mass (α)	Semi-major axis (β)	
		$dN/dM_{\text{P}} \propto (M_{\text{P}})^{\alpha}$	$dN/da \propto a^{\beta}$	
Direct Imaging	Present work	-1.31	-0.61	≤ 17.9 %
Direct Imaging	Lafrenière et al. 2007	-1.2	-1.0	≤ 9.3 %
Radial velocity	Cumming et al. 2008	-1.31	-0.61	10.5 ± 1.7 %
Microlensing	Cassan et al. 2012	-1.68	-1.0	17_{-9}^{+6} %

Our use of β is taken from Cumming et al. (2008). In direct imaging by Lafrenière et al. (2007), α and β were the values extrapolated from RV observations. Lafrenière et al. (2007) and Cassan et al. (2012) assumed a flat distribution in logarithmic semi-major axis space.

of $> |10|$ degrees in the imaging by Chauvin et al. (2010). Among them, 5 stars have already been confirmed as background objects while 78% remain to have their proper motion observed. It is highly likely that most of them are background stars, but we would like to point out that as a by-product, deep direct imaging would also be useful to discuss galactic models. This, however, is beyond the scope of our paper.

7. Summary

We have carried out a SEEDS imaging survey for detection of extrasolar gas-giant planets in the Pleiades with the near-infrared imaging instrument HiCIAO and the adaptive optics instrument AO188 on the Subaru telescope between October 2009 and January 2012. Thirteen companion candidates were found around 9 host stars in H band by using ADI observations. The detection limit of our observations (5σ) was 20.3 magnitudes with an integration time of 5–45 minutes beyond $1''.5$. For HD 23514 and HII 1348, we confirmed a brown dwarf respectively, which were detected by a previous study with proper motion measurement (Rodriguez et al. 2012; Geißler et al. 2012). Five of the 13 candidates were confirmed to be background stars on the basis of proper motion. One was not found in the second epoch observation; thus, this was unlikely to be a background or companion object. Only one it was not confirmed whether or not it is background star, as the precision of their proper motions was not sufficient. Four of the 13 remain to be observed to confirm whether they are co-moving.

We determined the detection efficiency, which is the probability of finding a 6–12 Jovian-mass planet at 50–1000 AU from the host star in the Pleiades, to be about 90% on the basis of our detection limit. Because there was no detection of such a planet, we estimated that the frequency of stars having gas-giant planets in the Pleiades is less than 17.9%. This result is consistent with previous direct imaging studies, indicating that planet frequency in the Pleiades is not considerably higher than those obtained in moving groups and field stars.

Appendix. Observation images

Details regarding the images and reduction are described in Table 2 and section 4. All images are obtained through ADI reduction in the H and K_S (only Figure 5(1); TYC 1800-2144-1). The field of view of all images is $19''.5 \times 19''.5$. The circle in images represents the position of the companion candidates (CCs).

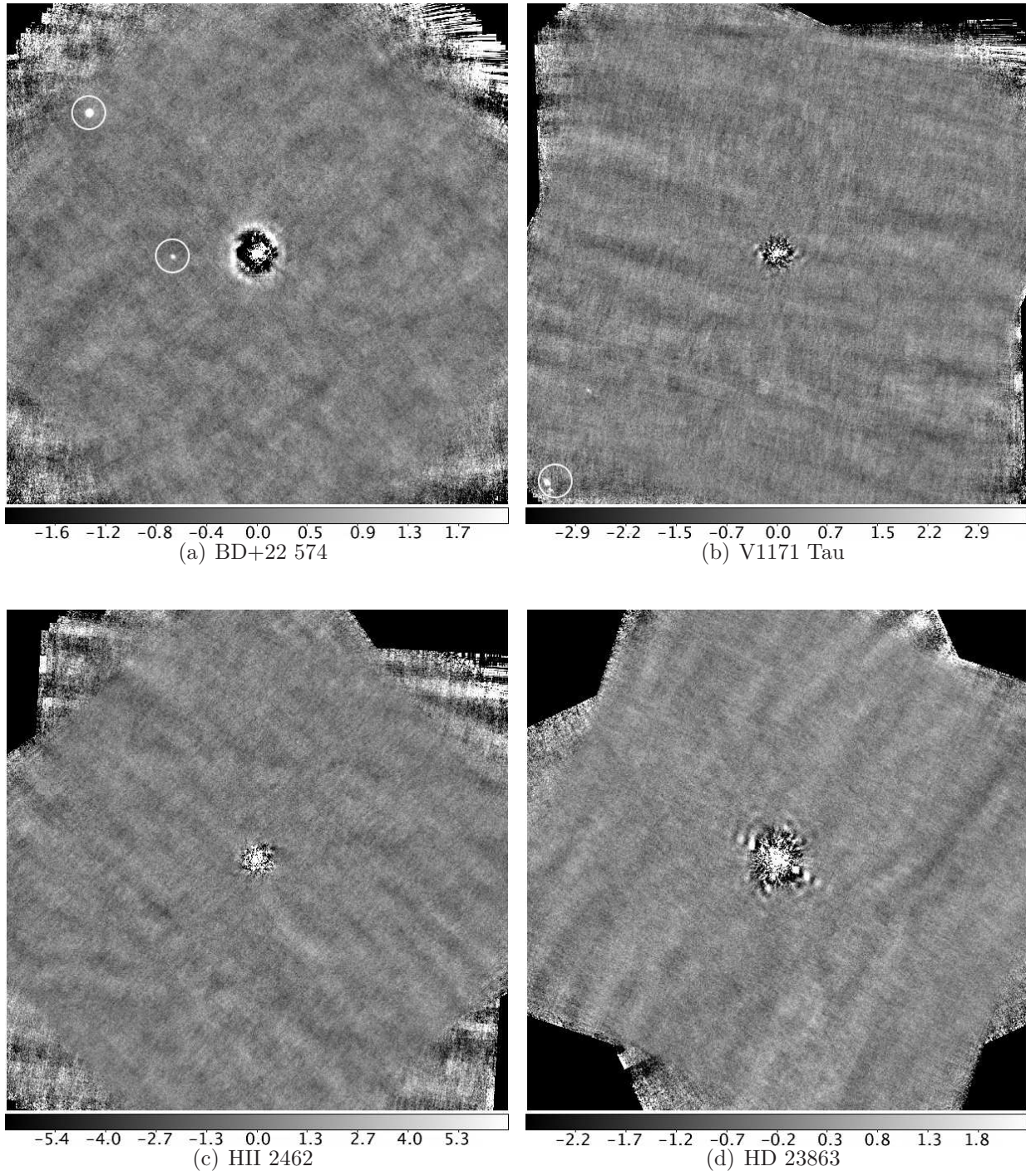


Fig. 5. *Top left panel:* BD+22 574. *Top right panel:* V1171 Tau. 2 CCs are in one circle. *Lower left panel:* HII 2462. *Lower right panel:* HD 23863. The unit of the color bar is ADU per each exposure time.

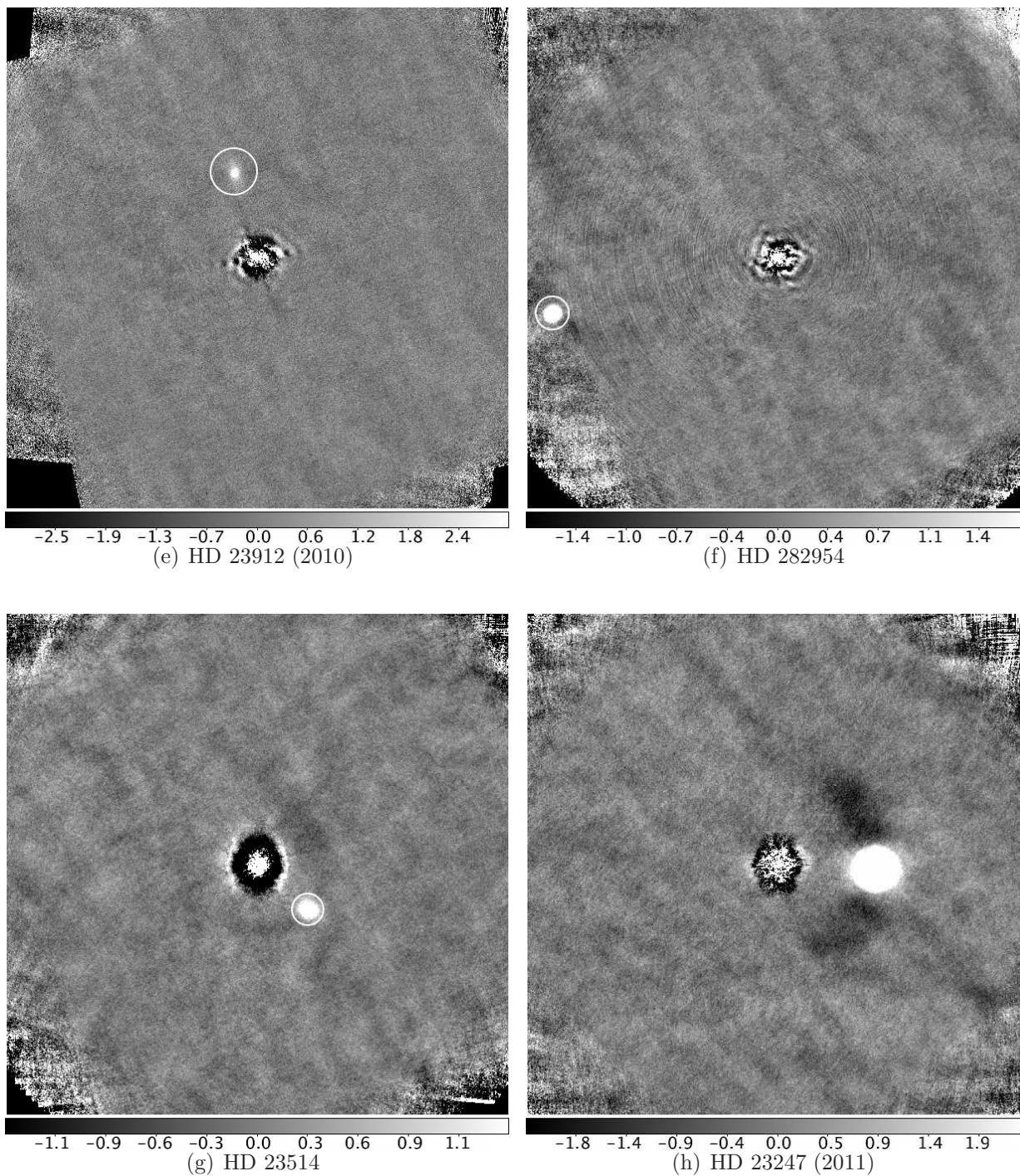


Fig. 5. *Continued.* *Top left panel:* HD 23912 (2010). *Top right panel:* HD 282954. *Lower left panel:* HD 23514. *Lower right panel:* HD 23247 (2011). The unit of the color bar is ADU per each exposure time.

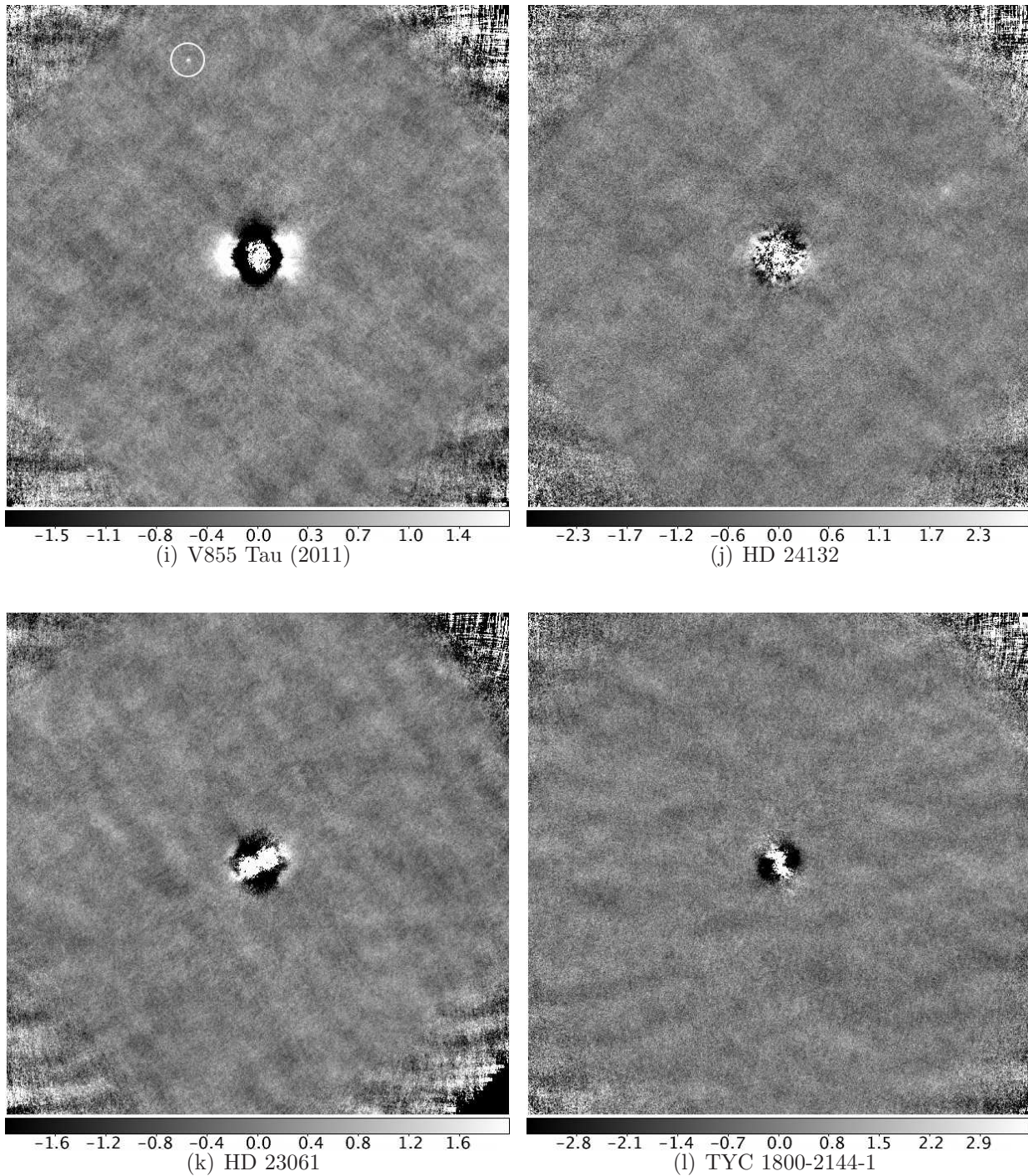


Fig. 5. *Continued.* Top left panel: V855 Tau (2011). Top right panel: HD 24132. Lower left panel: HD 23061. Lower right panel: TYC 1800-2144-1. The unit of the color bar is ADU per each exposure time.

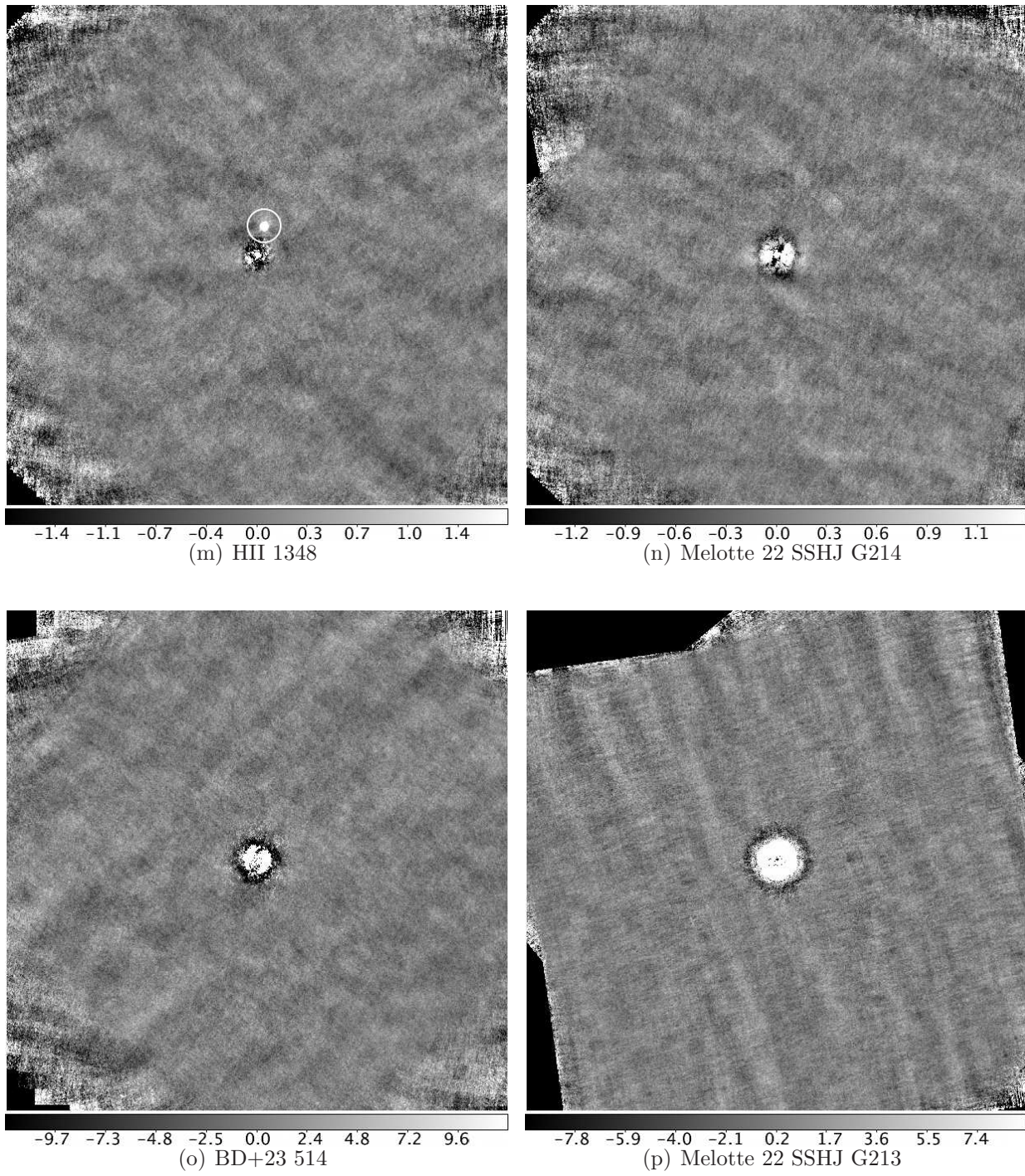


Fig. 5. *Continued.* Top left panel: HII 1348. Top right panel: Melotte 22 SSHJ G214. Lower left panel: BD+23 514. Lower right panel: Melotte 22 SSHJ G213. The unit of the color bar is ADU per each exposure time.

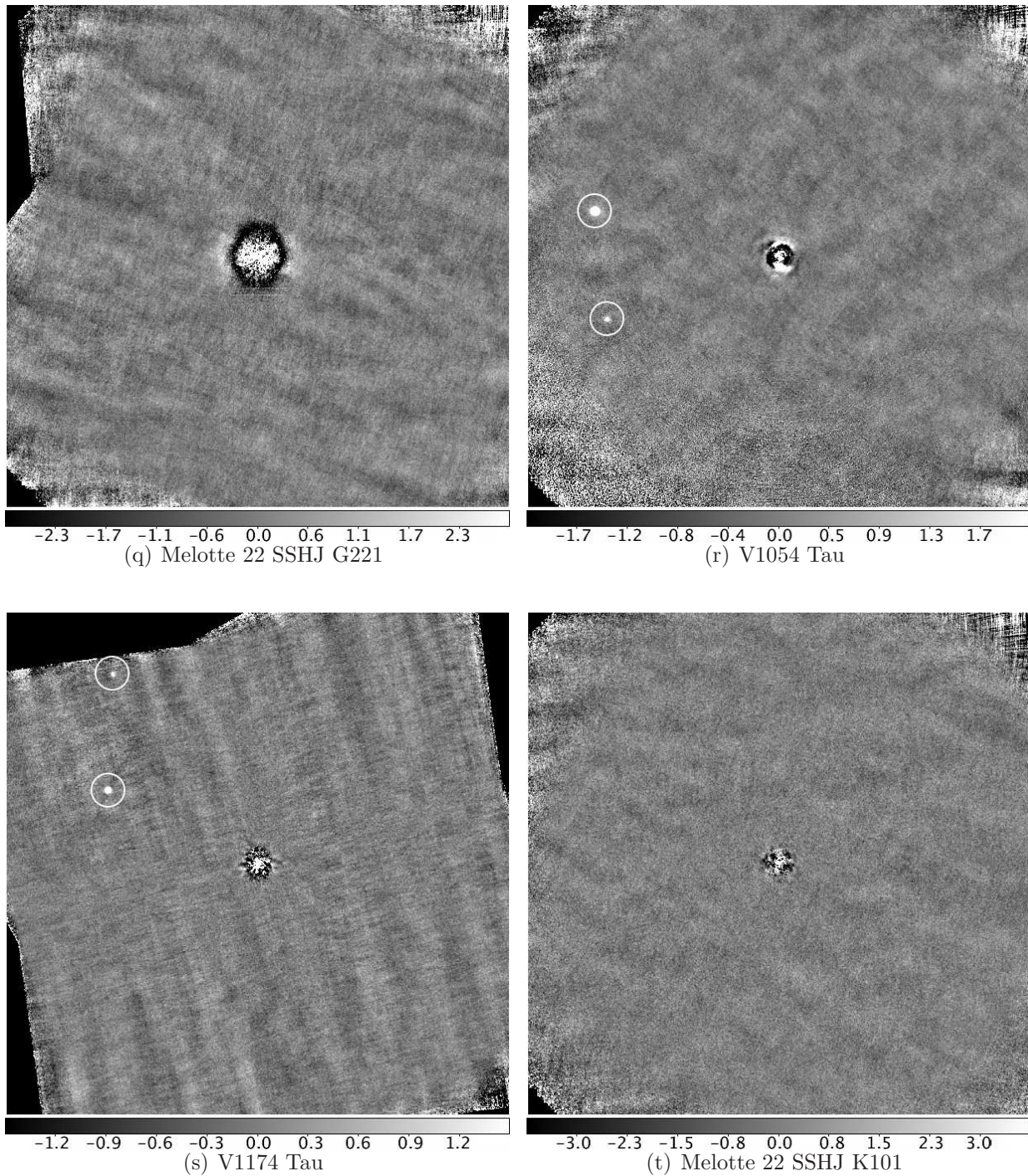


Fig. 5. *Continued.* Top left panel: Melotte 22 SSHJ G221. Top right panel: V1054 Tau. Lower left panel: V1174 Tau. Lower right panel: Melotte 22 SSHJ K101. The unit of the color bar is ADU per each exposure time.

References

- An, D., Terndrup, D. M., Pinsonneault, M. H., Paulson, D. B., Hanson, R. B., & Stauffer, J. R. 2007, *ApJ*, 655, 233
- Andrews, S. M., & Williams, J. P. 2007, *ApJ*, 659, 705
- Baraffe, I., Chabrier, G., Allard, F., & Hauschildt, P. H. 1998, *A&A*, 337, 403
- Baraffe, I., Chabrier, G., Allard, F., & Hauschildt, P. H. 2002, *A&A*, 382, 563
- Baraffe, I., Chabrier, G., Barman, T. S., Allard, F., & Hauschildt, P. H. 2003, *A&A*, 402, 701
- Basu, S., & Vorobyov, E. I. 2012, *ApJ*, 750, 30
- Beaulieu, J. P., et al. 2006, *Nature*, 439, 437
- Belikov, A. N., Hirte, S., Meusinger, H., Piskunov, A. E., & Schilbach, E. 1998, *A&A*, 332, 575
- Belikov, A. N., Kharchenko, N. V., Piskunov, A. E., Schilbach, E., Scholz, R. D., & Yatsenko, A. I. 2002, *A&A*, 384, 145
- Biller, B. A., et al. 2007, *ApJS*, 173, 143
- Bouvier, J., Rigaut, F., & Nadeau, D. 1997, *A&A*, 323, 139
- Cameron, A. G. W. 1978, *Moon Planets*, 18, 5
- Carson, J., et al. 2012, eprint arXiv:1211.3744
- Cassan, A., et al. 2012, *Nature*, 481, 167
- Chabrier, G., & Baraffe, I. 2000, *ARA&A*, 38, 337
- Chauvin, G., et al. 2010, *A&A*, 509, 52
- Cumming, A., Butler, R. P., Marcy, G. W., Vogt, S. S., Wright, J. T., & Fischer, D. A. 2008, *PASP*, 120, 531
- Currie, T., et al. 2011, *ApJ*, 729, 128
- Cutri, R. M., et al. 2003, 2MASS All Sky Catalog of Point Sources (The IRSA 2MASS All-Sky Point Source Catalog, NASA/IPAC Infrared Science Archive. <http://irsa.ipac.caltech.edu/applications/Gator/>)
- Fortney, J. J., Marley, M. S., Hubickyj, O., Bodenheimer, P., & Lissauer, J. J. 2005, *Astron. Nachr.*, 326, 925
- Fortney, J. J., Marley, M. S., Saumon, D., & Lodders, K. 2008, *ApJ*, 683, 1104
- Gratton, R. 2000, *ASPC*, 198, 225
- Geißler, K., Metchev, S. A., Pham, A., Larkin, J. E., McElwain, M., & Hillenbrand, L. A. 2012, *ApJ*, 746, 44
- Hayano, Y., et al. 2010, *Proc. SPIE*, 7736, 21
- Hodapp, K. W., et al. 2008, *Proc. SPIE*, 7014, 42
- Howard, A. W., et al. 2010, *Science*, 330, 653
- Ida, S. & Lin, D. N. C. 2004, *ApJ*, 604, 388
- Inutsuka, S., Machida, M. N., & Matsumoto, T. 2010, *ApJ*, 718, 58
- Itoh, Y., et al. 2005, *ApJ*, 620, 984
- Itoh, Y., Oasa, Y., Funayama, H., Hayashi, M., Fukagawa, M., Hashiguchi, T., & Currie, T. 2011, *Research in Astron. Astrophys.*, 11, 335
- Janson, M., Bonavita, M., Klahr, H., & Lafrenière, D. 2012, *ApJ*, 745, 4

- Kouwenhoven, M. B. N., Goodwin, S. P., Parker, R. J., Davices, M. B., Malmberg, D., & Kroupa, P. 2010, *MNRAS*, 404, 1835
- Kratter, K. M., Murray-Clay, R. A., & Youdin, A. N. 2010, *ApJ*, 710, 1375
- Kubas, D., et al. 2008, *A&A*, 483, 317
- Kuiper, G. P. 1951, *Proc. Natl. Acad. Sci.*, 37, 1
- Lafrenière, D., et al. 2007, *ApJ*, 670, 1367
- Lagrange, A.-M., et al. 2010, *Science*, 329, 57
- Liu, M. C. 2004, *Science*, 305, 1442
- Lodieu, N., Dobbie, P. D., Deacon, N. R., Hodgkin, S. T., Hambly, N. C., & Jameson, R. F. 2007, *MNRAS*, 380, 712
- Marley, M. S., Fortney, J. J., Hubickyj, O., Bodenheimer, P., & Lissauer, J. J. 2007, *ApJ*, 655, 541
- Marois, C., Lafrenière, D., Doyon, R., Macintosh, B., & Nadeau, D. 2006, *ApJ*, 641, 556
- Marois, C., Macintosh, B., Barman, T., Zuckerman, B., Song, I., Patience, J., Lafrenière, D., & Doyon, R. 2008, *Science*, 322, 1348
- Marois, C., Zuckerman, B., Konopacky, Q. M., Macintosh, B., & Barman, T. 2010, *Nature*, 468, 1080
- Masciadri, R., Mundt, R., Henning, Th., Alvarez, C., & Barrado y Navascues, D. 2005 *ApJ*, 625, 1004
- Masset, F. S., & Papaloizou, J. C. B. 2003 *ApJ*, 588, 494
- Mayor, M., et al. 2011, *arXiv*, 1109.2497
- Micela, G., Sciortino, S., Kashyap, V., Harnden, F. R., Jr., & Rosner, R. 1996, *ApJS*, 102, 75
- Mizuno, H. 1980, *Prog. Theor. Phys.*, 64, 544
- Nielsen, E. L., & Close, L. M. 2010, *ApJ*, 717, 878
- Pinfield, D. J., Dobbie, P. D., Jameson, R. F., Steele, I. A., Jones, H. R. A., & Katsiyannis, A. C. 2003, *MNRAS*, 342, 1241
- Pollack, J. B., Hubickyj, O., Bodenheimer, P., Lissauer, J. J., Podolak, M., & Greenzweig, Y. 1996, *Icarus*, 124, 62
- Raboud, D., & Mermilliod, J.-C. 1998, *A&A*, 329, 101
- Rafikov, R. R. 2007, *ApJ*, 662, 642
- Rafikov, R. R. 2011, *ApJ*, 727, 86
- Rodriguez, D. R., Marois, C., Zuckerman, B., Macintosh, B., & Melis, C. 2012, *ApJ*, 748, 30
- Soderblom, D. R., Nelan, E., Benedict, G. F., McArthur, B., Ramirez, I., & Spiesman, W. 2005, *AJ*, 129, 1616
- Safronov, V. 1969, *Evolution of the Protoplanetary Cloud and Formation of the Earth and Planets*
- Skiff, B. A. 2010, *VizieR Online Data Catalog*, 1, 2023
- Spiegel, D. S., & Burrows, A. 2012, *ApJ*, 745, 174
- Stauffer, J. R., Schultz, G., & Kirkpatrick, J. D. 1998, *ApJ*, 499, 199
- Stauffer, J. R., et al. 2007, *ApJS*, 172, 663
- Sumi, T., et al. 2010, *ApJ*, 710, 1641
- Suzuki, R., et al. 2010, *SPIE*, 7735.101S
- Tamura, M. 2009, *American Institute of Physics Conference Series*, 1158, 11
- van der Marel, R. P., Gerssen, J., Guhathakurta, P., Peterson, R. C., & Gebhardt, K. 2002, *AJ*, 124, 3255

van Leeuwen, F. 2009, A&A, 497, 209

Veras, D., Crepp, J., & Ford, E. B. 2009, ApJ, 696, 1600

Vigan, A., et al. 2012, A&A, 544, 9

Wright, C. O., Egan, M. P., Kraemer, K. E., & Price, S. D. 2003, AJ, 125, 359

Zacharias, N., Monet, D. G., Levine, S. E., Urban, S. E., Gaume, R., & Wycoff, G. L. 2004, A&AS, 205,4815